ISSN 1068-1620, Russian Journal of Bioorganic Chemistry, 2024, Vol. 50, No. 4, pp. 1491–1511. © Pleiades Publishing, Ltd., 2024.

Spectral Characterization, Antioxidant, Antibacterial Activity, and Molecular Dynamics Simulation of a New Bis-benzimidazole Molecule, 1,5-Bis(1*H*-benzimidazol-2-yl)pentan-3-one

T. Karakurt[a], A. Tavman[b,*], O. Şahin[c], D. N. Çolak[d], and A. A. Karaçelik[e]

[a] *Kırsehir Ahi Evran University, Faculty of Engineering-Architecture, Department of Chemical Engineering, Kırsehir, 40100 Turkey*
[b] *Istanbul University-Cerrahpaşa, Faculty of Engineering, Department of Chemistry, Avcilar, Istanbul, 34320 Turkey*
[c] *Sinop University, Faculty of Health Sciences, Department of Occupational Health and Safety, Sinop, 57000 Turkey*
[d] *Giresun University, Dereli Vocational School, Department of Forestry, Giresun, 28950 Turkey*
[e] *Giresun University, Espiye Vocational School, Giresun, 28600 Turkey*
**e-mail: atavman@iuc.edu.tr*

Received December 10, 2023; revised December 23, 2023; accepted December 24, 2023

Abstract—Objective: Bis-benzimidazoles are an interesting class of compounds due to their chelating characteristics, various biological effects, and fluorescence properties. **Methods:** In this research, a new symmetric bis-benzimidazole derivative including a ketone group, 1,5-bis(1*H*-benzimidazol-2-yl)pentan-3-one (**PBB**), was synthesized and characterized. Antibacterial activity of PBB was tested against Gram-negative and Gram-positive bacteria. The total antioxidant capacity (as TEAC value) and free radical scavenging activity of (**PBB**) was determined by ferric reducing antioxidant power (FRAP) and 1,1-diphenyl-2-picrylhydrazyl (DPPH) methods. Molecular modeling methods have been conducted in order to study the relationship between electronic characteristics and antioxidant activity. **Results and Discussion:** Molecular modelling techniques and approaches were used to ensure that (**PBB**) synthesized in this study could be a reliable drug-like ligand, ligand-protein interactions were studied in detail with molecular dynamic (MD) simulation techniques applied at the molecular level, and trajectory analyses after MD were discussed. The total antioxidant capacity (as TEAC value) and free radical scavenging activity results revealed that (**PBB**) has a moderate inhibition with a SC_{50} = 1.8686 ± 0.0030 mg/mL value and the FRAP value is 108.89 ± 1.92 μM TEAC. **Conclusions:** According to the molecular modelling calculations, the antioxidant and antibacterial activities of (**PBB**) result from the electrophilic and nucleophilic interactions of its electron-rich C=N nitrogen atoms and electron-withdrawing carbon atoms adjacent to the C=O group with the proteins of the target molecules.

Keywords: bis-benzimidazole, X-ray crystal, computational study, molecular modelling, antioxidant activity

DOI: 10.1134/S1068162024040253

INTRODUCTION

Benzimidazole is an attractive heterocyclic ring because it is present in cyanocobalamin (vitamin B12) and various drugs such as omeprazole, albendazole, mebendazole etc. It is also plays a role in clinically confirmed antivirals, antihistamines, anthelmintics, and antiulcers [1]. There are a lot of studies about benzimidazole derivatives that exhibit antitumor and antimicrobial properties and act as thrombopoietin receptor agonists [2–11].

Bis-benzimidazoles have attracted attention because of the coordination of the double bonded heterocyclic ring nitrogen atom (–C=N–), which acts as a ligand in transition metal complexes [12–19]. They give chelate complexes coordinating through both the C=N nitrogen atoms [12, 20] and have metallic polymer forming

characteristics as typical multidentate ligands [21]. In addition, it was reported that bis-benzimidazoles showed significant antimicrobial activities such as antibacterial and antifungal [22–25] and anticancer effect [26].

Studies on the antioxidant effects of bis-benzimidazole compounds and metal complexes of some of them are available in the literature [27, 28]. For example, Ouaket et al. investigated antioxidant activity of 2,2′-octane-1,8-diylbis(1*H*-benzimidazole), 2,2′-benzene-1,4-diylbis(1*H*-benzimidazole), and their 5-amino/nitro derivatives and 2,2′-alkyl/aryl-bis(8-quinolinol-5-azobenzimidazole) against oxidative (H_2O_2) and nitrosative (SNP) stress using the protozoan *T. thermophila* as a cellular model [29, 30]. It was reported that 1,2-bis(1-methyl-1*H*-benzo[*d*]imidazol-2-ylthio)ethane and its dicationic analogue show good results in hydrogen peroxide scavenge assay [31]. It was reported that Ag(I) complex of 1,3-bis(1-methyl-benzimidazol-2-yl)-2-thiapropane [32], Cu(II) complexes of 1,3-bis(1-ethylbenzimidazol-2-yl)-2-thiapropane [33], and 1,3-bis(1-allylbenzimidazol-2-yl)-2-oxapropane [34] possessed significant antioxidant activity against superoxide ($O_2^{\cdot-}$) and hydroxyl ($OH^{\cdot}$) radicals. Mn(II) and Co(II) complexes with bis(benzimidazol-2-ylmethyl)-allylamine displayed high scavenging activity against hydroxyl and superoxide radicals [35]. Antioxidant activity of 1,3-bis(1-methyl/butylbenzimidazol-2-yl)-2-oxapropanes and their Cu(II) complexes was studied by Wu et al. [36, 37]. Bis(*N*-ethylbenzimidazol-2-ylmethyl)allylamine and its Mn(II) and Zn(II) complexes were investigated and found that Mn(II) complex exhibited potential antioxidant properties [38]. It was reported that three Cu(II) ternary complexes of bis(2-benzimidazolylmethyl)amine possessed significant antioxidant activities [39]. 1,3-Bis(1-ethyl/benzyl/allyl-benzimidazol-2-yl)-2-oxapropanes and their Ag(I) complexes were investigated and Ag(I) complex of benzyl derivative showed high_antioxidant activity [40]. Antioxidant activity of Ag(I) complexes of bis(2-benzimidazol-2-ylmethyl)benzylamine and its *N*-methyl/benzyl derivatives were also reported [41].

There are limited studies on bis-benzimidazoles including keto group. We reported preparation and spectral characterization of 1,3-bis(1*H*-benzimidazol-2-yl)-propan-1-one that an asymmetric bis-benzimidazole and its various complexes with Zn(II) salts [42]. Synthesis and some properties of bis(1*H*-benzimidazol-1-yl)-methanone [43–45] and bis(1-methyl-1*H*-benzimidazol-1-yl)-methanone and its Cu(II) complex was reported [46]. Ketonization of methylene of bis(benzimidazol-2-yl)methane by molecular oxygen under the catalysis of cobalt(II) ion was reported [47]. Bis(1-methylbenzimidazol-2-yl)ketone was synthesized by lithiation of 1-methylbenzimidazole and its Cu(I) and Cu(II) complexes were prepared by Gorun et al. [48].

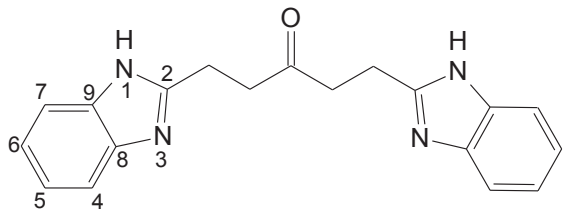

Fig. 1. Chemical structure of 1,5-bis(1*H*-benzimidazol-2-yl)-pentan-3-one (**PBB**).

In this study, a new bis-benzimidazole derivative, 1,5-bis(1*H*-benzimidazol-2-yl)pentan-3-one ((**PBB**), Fig. 1) is synthesized and characterized by physicochemical, and spectroscopic techniques. Then, molecular modeling techniques and approaches were used to ensure that a new (**PBB**) compound synthesized in this study could be a reliable drug-like ligand, ligand-protein interactions were studied in detail with MD simulation techniques applied at the molecular level, and trajectory analyses after MD were discussed. In addition, antibacterial and antioxidant activities of the obtained compounds were investigated. This study can be considered as the first example of a ketonic bis-benzimidazole compound in this field.

RESULTS AND DISCUSSION

Chemistry

1,5-Bis(1*H*-benzimidazol-2-yl)pentan-3-one (**PBB**) was synthesized by known method [49] and characterized by ^{1}H and ^{13}C NMR, FT-IR, fluorescence spectroscopy, and mass spectrometry (Experimental section).

The experimental FT-IR spectra of benzimidazoles give a strong or medium band in the region 3400–3250 cm^{-1} corresponding to the stretching vibration of NH group [50]. In our study, this band is appeared at 3283 cm^{-1} as medium characteristic (Fig. S1, supplementary information). The bands at 3108 and 3056 cm^{-1} belong to aromatic stretching vibrations, and a strong sharp band at 739 cm^{-1} indicating o-substitution of out-of-plane C–H bending. The medium bands around 2900 cm^{-1} are due to the aliphatic CH_2 groups. A medium intense band at 1629 cm^{-1} is assigned to the ν(C=N) stretch. The stretching vibrations of aromatic C=C bonds are detected at 1598 cm^{-1} as medium characteristic. The C=O is a very characteristic group for the title compound and is detected at the wavenumber 1708 cm^{-1} as strong band.

The protons H4 and H7 appear at 7.46 ppm, H5 and H6 at 7.11 ppm as singlet in ^1H NMR spectra. The CH_2 protons of the bridging group ($–CH_2–CH_2–)_2C=O$) near the imidazole ring were detected at 3.11 ppm as broad doublet, the other CH_2 protons (next the C=O group) at 3.06 ppm as broad doublet (Fig. S2, supplementary information). The signal of the NH proton could not be detected due to very fast fluxional behavior in the solvent, namely DMSO-d_6. The C=O and C2 carbon atoms are appear at 208.70 and 155.0 ppm, respectively (Fig. S3, supplementary information).

One of the major characteristics of the benzimidazole derivatives is to have fluorescence property. Likewise, (**PBB**) shows fluorescence characteristic. Fluorescence spectrum of (**PBB**) was obtained in ethanol solution at room temperature (excitation wavelength: 354 nm; concentration: 1×10^{-4} mol/L). The emission spectral data are presented in Experimental section. Three emission bands were observed in the fluorescence spectrum of (**PBB**) (triple fluorescence): 394 (m), 421 (m, br), and 458 (m, br) nm. These bands probably result from the following factors: 1) the normal Stokes shift originating from a locally excited π* electronic state (458 nm); 2) intramolecular charge transfer (421 nm), and 3) monocation protonated at the benzimidazole nitrogen atom N3 as a result of an interaction (394 nm), such as hydrogen bonding, with the solvent (ethanol) [51, 52].

X-Ray Diffraction Analysis

Crystal data and structure refinement parameters are given in Table 1; selected bond distances and angles for (**PBB**) are shown in Table 2. The optimized structure of (**PBB**) is shown in Fig. 2; the molecular structure of (**PBB**) with the atom labelling is shown in Fig. 3. The O1–C10 bond is typical double bond character with a 1.202 (5) Å bond length. The dihedral angle between benzimidazole rings is 81.49 (6)°. Each benzimidazole ring plane is approximately planar, with maximum deviation from the least-squares plane being 0.0160 (35) Å for atom C2 and 0.0175 (34) Å for atom C19. The molecules of (**PBB**) are connected by N–H···N hydrogen bonds and C–H···π interactions (Table 3). Atoms N2 and N4 acts as H-bond donors, via atom H2A and H4A, to atoms N1 and N3 in the molecule at x, –y + 3/2, z + 1/2,

Table 1. Crystal data and structure refinement parameters for (**PBB**)

Data	
Empirical formula	$C_{19}H_{18}N_4O$
Formula weight	318.37
Crystal system	Monoclinic
Space group	$P2_1/c$
a (Å)	19.853 (3)
b (Å)	8.1251 (11)
c (Å)	10.2818 (12)
b	100.639 (5)
V (Å^3)	1630.0 (4)
Z	4
D_c (g cm^{-3})	1.297
μ (mm^{-1})	0.08
θ range (°)	3.1–28.3
Measured refls.	28435
Independent refls.	3937
R_{int}	0.056
S	1.25
R1/wR2	0.103/0.214
D	0.34/–0.26
CCDC	1832838

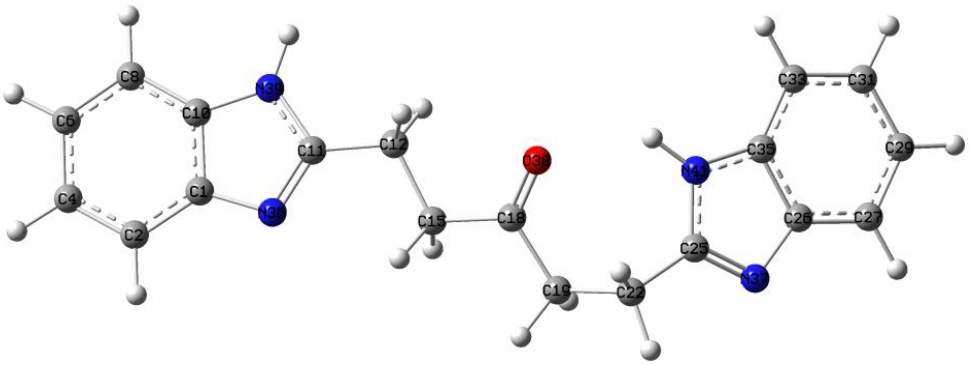

Fig. 2. Optimized structure of (**PBB**) compound.

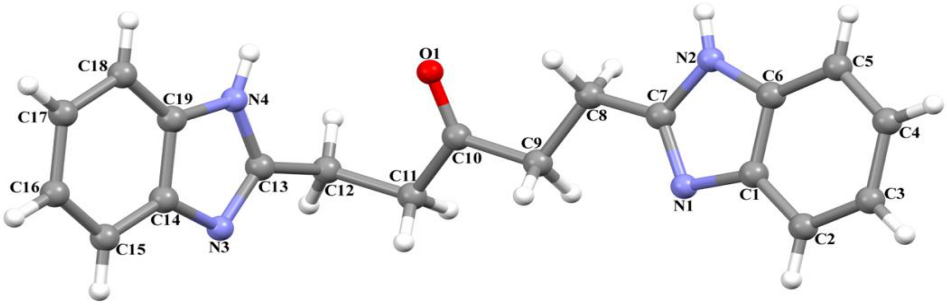

Fig. 3. The molecular structure of (**PBB**) showing the atom numbering scheme.

Table 2. Selected bond distances and angles for (**PBB**)

Bond	Distances (Å, °)	Bond	Distances (Å, º)
C10–O1	1.202 (5)	C13–C12	1.486 (6)
C12–C11	1.522 (5)	C11–C10	1.503 (5)
C10–C9	1.523 (5)	C8–C9	1.508 (5)
C8–C7	1.480 (5)	C13–N4	1.361 (5)
C13–N3	1.316 (5)	C7–N2	1.359 (5)
C7–N1	1.327 (5)	C6–N2	1.387 (5)
C9–C10–C11	116.2 (3)	C10–C11–C12	114.0 (3)
C9–C10–O1	121.9 (4)	C11–C10–O1	121.9 (4)
C10–C11–C12–C13	–73.3 (5)	C7–C8–C9–C10	168.9 (4)
C12–C11–C10–O1	–6.7 (6)	C8–C9–C10–O1	–15.6 (6)

Table 3. Hydrogen bonds parameters for (**PBB**) (Å, °)

D–H···A	D–H	H···A	D···A	D–H···A
N2–H2A···N1^{i}	0.83 (4)	2.17 (4)	2.974 (4)	163
N4–H4A···N3^{i}	0.84 (4)	2.11 (4)	2.935 (4)	168
C4–H4···Cg(2)^{ii}	0.93	2.88	3.643 (5)	140
C9–H9A···Cg(3)^{ii}	0.97	2.95	3.687 (5)	133

Symmetry codes: (*i*) x, –y + 3/2, z + 1/2; (*ii*) 1–x, 1–y, 1–z; Cg(2) = N3/N4/C13/C14/C19; Cg(3) = C1–C6.

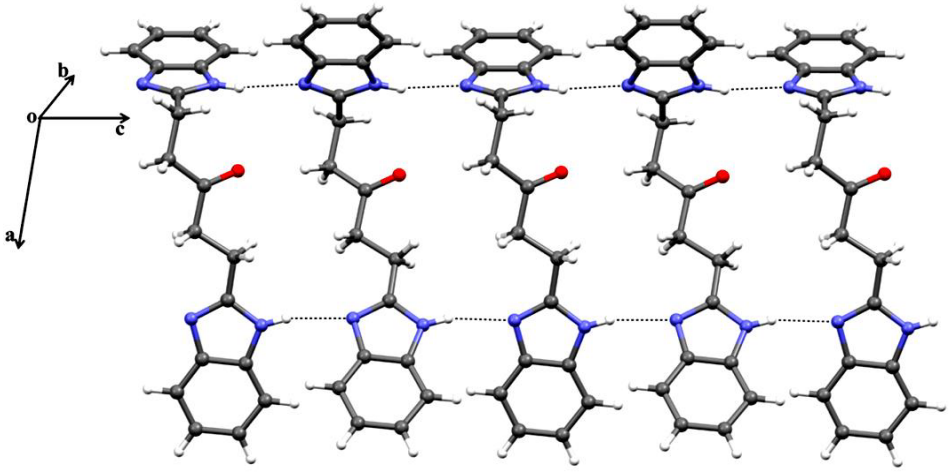

Fig. 4. Part of the crystal structure of (**PBB**), showing the formation of edge-fused $R_2^2(20)$ rings.

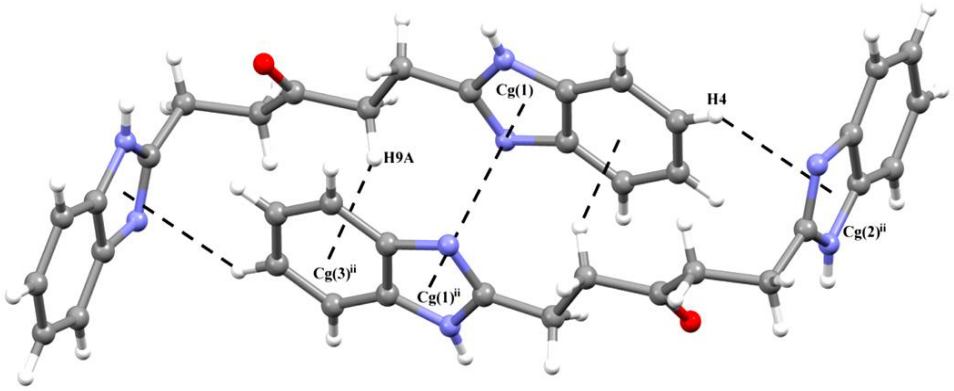

Fig. 5. Part of the crystal structure of (**PBB**), showing the formation of C–H···π and π···π interactions.

forming a C(4) chains running parallel to the [001] direction. The combination of C (4) chains produce edge-fused R_2^2 (20) rings (Fig. 4). Atom C9 in the molecule at x, y, z acts as hydrogen-bond donor to the C1–C6 phenyl ring in the molecule at 1–x, 1–y, 1–z, so forming a centrosymmetric $R_2^2(14)$ ring centered at 1/2, 1/2, 1/2 (Fig. 5). Compound (**PBB**) also contains one π···π interaction. An intermolecular π···π contact occurs between the two symmetry-related imidazole rings of adjacent molecules (Fig. 5). The distance between the ring centroids is found as 3.992 (2) Å.

Quantum Chemical Activity Indicatives and Molecular Docking

Frontier orbitals (FMOs) and molecular electrostatic potential (MEP) surface scanning were performed to determine the nucleophilic and electrophilic sites with biological activity in molecular docking studies of the optimized ligands. FMO theory states that HOMO orbitals are donor and LUMO orbitals are acceptor sites [53, 54]. These orbitals can be used to interpret studies to determine the binding sites of the ligand and receptor complex. As shown in Fig. 6, the HOMO

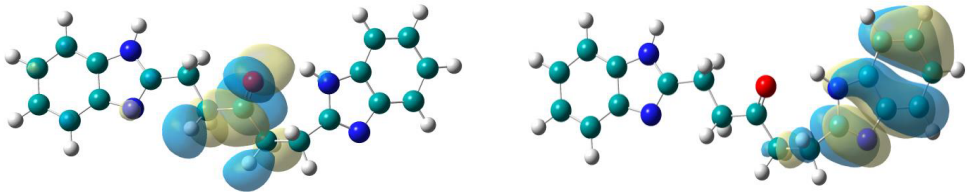

Fig. 6. HOMO-LUMO orbitals of (**PBB**) compound.

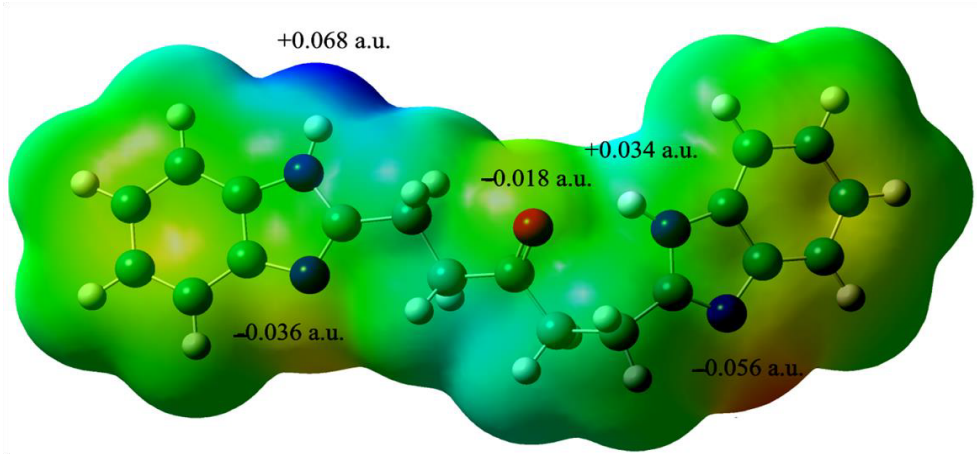

Fig. 7. MEP maps of (**PBB**) compound.

orbitals are localized around the N41, N37 atoms, and the benzimidazole ring, while the LUMO orbitals are located on the C=O and adjacent CH_2 groups. These results suggest that these regions of (**PBB**) may play important roles in antioxidant activity.

Molecular electrostatic potential (MEP) surface scanning is another method used to determine the active sites of the ligand to be used in drug design. In Fig. 7, the MEP surface map of (**PBB**) compound shows that the red colored regions are partially negative charge or electron rich and the blue colored regions are partially positive charge or electron deficient regions. It is seen that the negative regions are mostly on the electronegative atoms N36, N37, and O38 and the positive regions are on the H atoms of N–H groups. Especially the red color of the regions on benzene rings indicates that these regions may be involved in hydrophobic interaction in the binding of the ligand with the receptor.

EGFR is a transmembrane glycoprotein consisting of an extracellular ligand binding domain and a cytoplasmic tyrosine kinase domain. EGFR acts as an important mediator in cell signaling pathways involving cell proliferation and metastatic spread [55]. The target protein structure (PDB ID: 7JXQ; EGFR kinase (T790M/V948R) in complex with allosteric inhibitor JBJ-09-063) and related data were retrieved from the "Protein Databank" for docking search. JBJ-09-063 (coligand) has been used in trials examining the treatment of cancer, glioblastoma multiforme, brain, and central nervous system tumours [56]. Autodockvina programme in Chimera was used to prepare the ligands and protein for docking and to dock the ligands to the protein. The complex structure resulting from the calculation was visualized using BIOVA DS Visualizer software (DSV). The ligands used in the study were successfully inserted into the active site of the receptor (Figs. 8 and 9). The properties of ligand-receptor interactions are given in Tables 4 and 5.

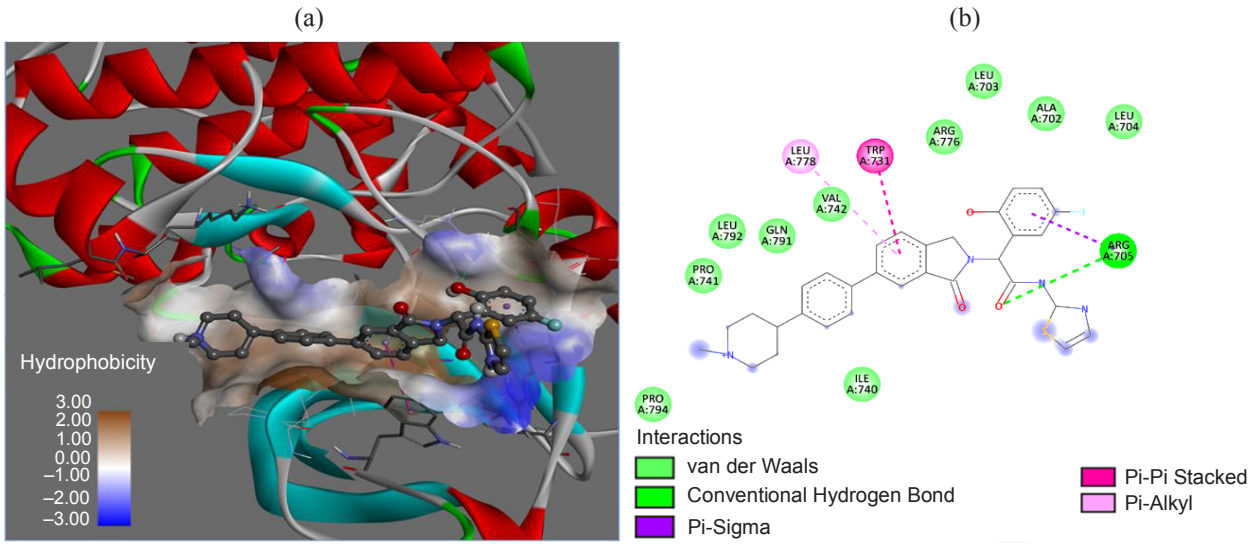

Fig. 8. (a) The position of the coligand located in the active area of the receptor in the complex structure mapped with the electrostatic potential and (b) two-dimensional coligand-receptor interaction diagram.

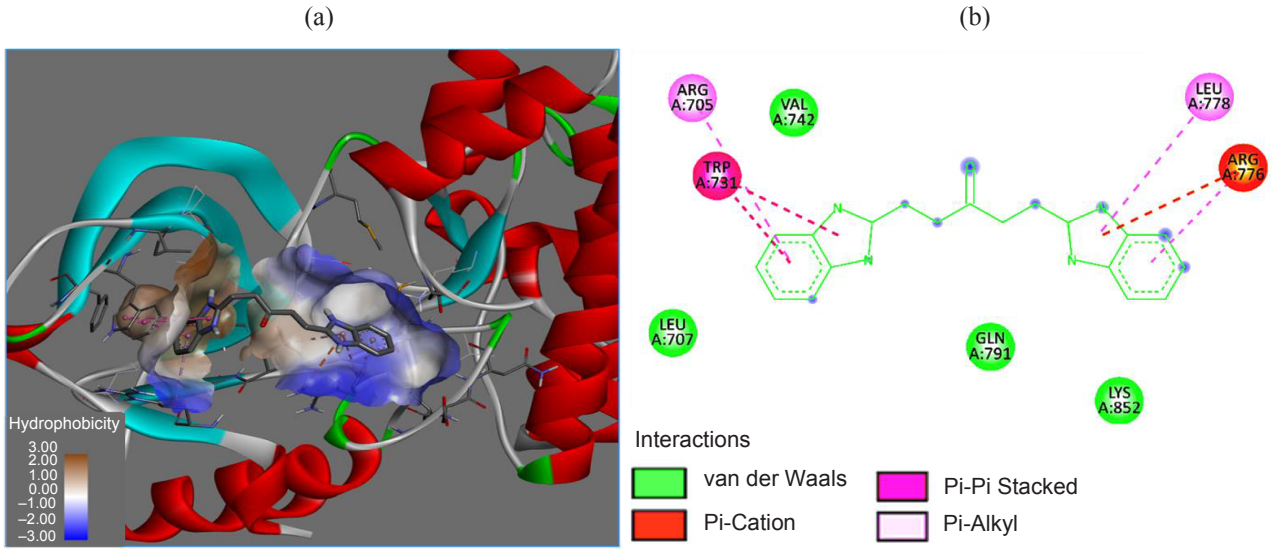

Fig. 9. (a) The position of (**PBB**) ligand located in the active site of the receptor in the complex structure mapped with the electrostatic potential and (b) two-dimensional PBB-receptor interaction diagram.

The 4-fluorophenol ring groups of the coligand compound and the benzimidazole ring groups of (**PBB**) are located in the hydrophobic pocket in the deep cavity of the receptor. The coligand is located almost parallel to the TRP731 residue and almost perpendicular to LEU778. It formed a π–π stacking interaction with TRP731 and a T-shaped Pi-alkyl interaction with LUE778 (Fig. 10a). The 4-fluorophenol ring group of the coligand also hydrogen bond with ARG705. Compound (**PBB**) is located almost parallel to the TRP731 residue. Compound (**PBB**) made π–π stacking interaction with TRP731 and T-shaped Pi-alkyl interaction with ARG705, LEU778, and ARG776 (Fig. 10b). The higher binding energy of (**PBB**) compared to the coligand was interpreted to be due to more interactions with the receptor. Both ligands were found to bind to the active site of the target in a geometry almost perpendicular to each other.

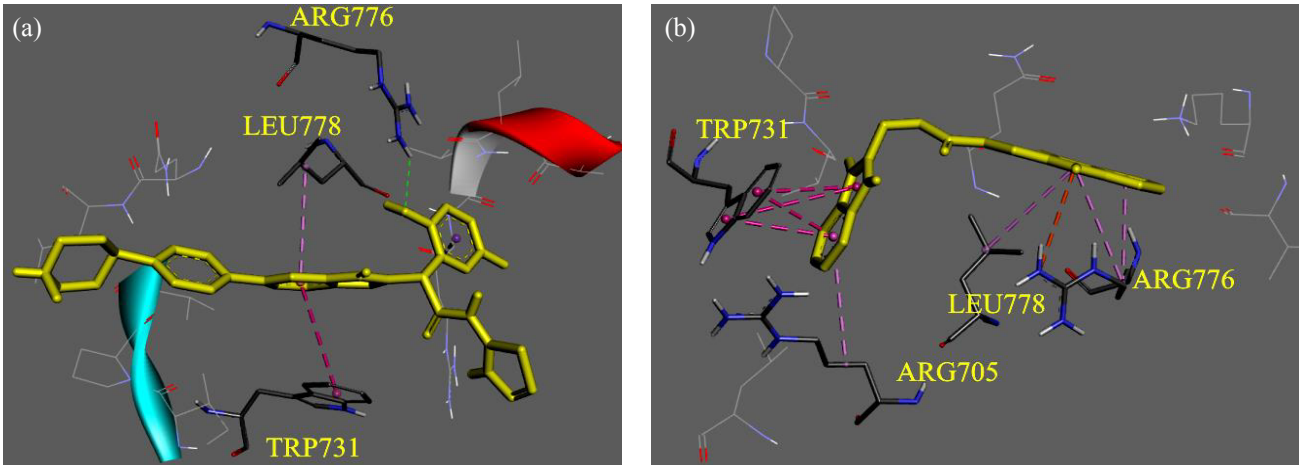

Fig. 10. (a) Coligand and (b) binding interaction of (**PBB**) with amino acid residues of the target.

Table 4. Interactions between coligand and **7JXQ** receptor

Name	Distance	Interaction	Types	Donor group	Donor atom	Acceptor group	Acceptor atom
A:ARG776:HH21—coligand:O	2.47034	H-bond	Conventional	A:ARG776	HH21	coligand	O
A:ARG705:CB—coligand	3.88	Hydrophobic	Pi-Sigma	A:ARG705:CB	C–H	coligand	Pi-Orbitals
A:TRP731—coligand	5.04421	Hydrophobic	Pi-Pi Stacked	A:TRP731	Pi-Orbitals	coligand	Pi-Orbitals
coligand—A:LEU778	5.28683	Hydrophobic	Pi-Alkyl	coligand	Pi-Orbitals	A:LEU778	Alkyl

Table 5. Interactions between (**PBB**) and **7JXQ** receptor

Name	Distance	Interaction	Types	Donor group	Donor atom	Acceptor group	Acceptor atom
A:ARG776:NH_2—**PBB**	4.88147	Electrostatic	Pi-Cation	A:ARG776:NH_2	Positive	(**PBB**)—	Pi-Orbitals
A:TRP731—**PBB**	5.11593	Hydrophobic	Pi-Pi Stacked	A:TRP731	Pi-Orbitals	(**PBB**)—	Pi-Orbitals
A:TRP731—**PBB**	4.14701	Hydrophobic	Pi-Pi Stacked	A:TRP731	Pi-Orbitals	(**PBB**)—	Pi-Orbitals
A:TRP731—**PBB**	3.83878	Hydrophobic	Pi-Pi Stacked	A:TRP731	Pi-Orbitals	(**PBB**)—	Pi-Orbitals
(**PBB**)—A:TRP731	4.17678	Hydrophobic	Pi-Pi Stacked	(**PBB**)—	Pi-Orbitals	A:TRP731	Pi-Orbitals
(**PBB**)—	4.06628	Hydrophobic	Pi-Alkyl	(**PBB**)—	Pi-Orbitals	A:ARG776	Alkyl
(**PBB**)—	5.05572	Hydrophobic	Pi-Alkyl	(**PBB**)—	Pi-Orbitals	A:ARG776	Alkyl
(**PBB**)—	4.9466	Hydrophobic	Pi-Alkyl	(**PBB**)—	Pi-Orbitals	A:LEU778	Alkyl
(**PBB**)—	5.39131	Hydrophobic	Pi-Alkyl	(**PBB**)—	Pi-Orbitals	A:ARG705	Alkyl

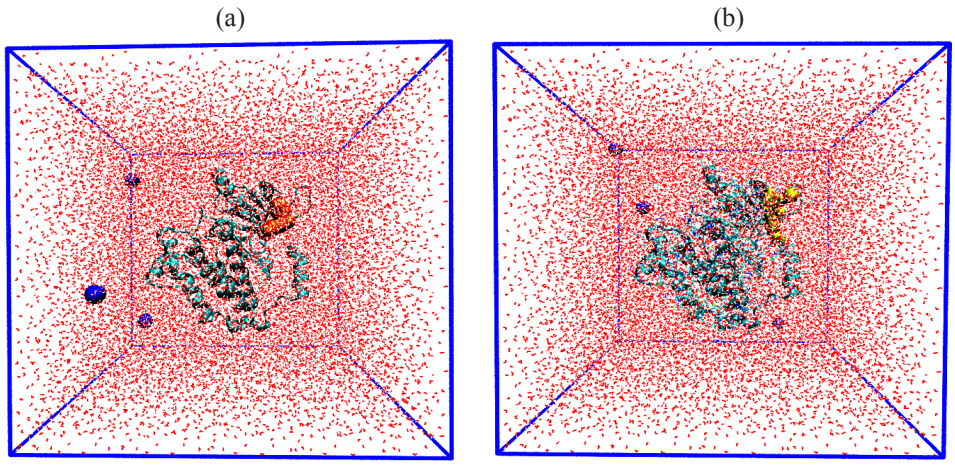

Fig. 11. System filled with water, neutralized with (a) coligand (orange), (b) (**PBB**) (yellow), and Cl^- ions (blue).

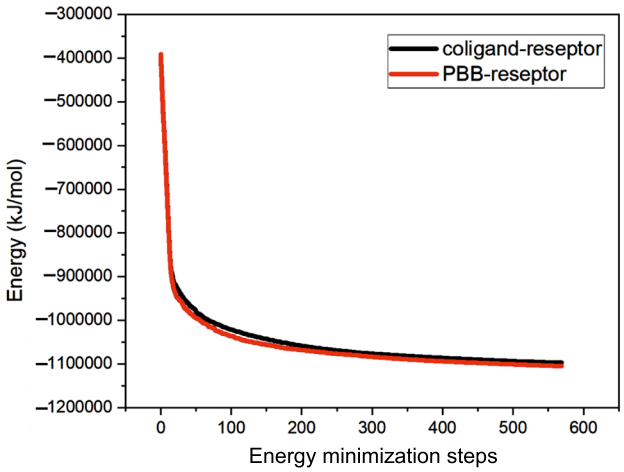

Fig. 12. Potential energy change of the system (protein + water + ions) obtained by energy minimization.

Molecular Dynamics

The complex structures obtained as a result of docking simulations were converted into "mol" format by making charge distributions in USCF Chimera software [57]. After the preparation of receptor-ligand complexes, molecular dynamics simulation was performed. AMBER [58] package program was used for protein model preparation, molecular dynamics studies, and analysis. Antechamber tools in the AMBER package program were used to convert the mol2 files of the ligands to GAFF (General Amber Force Field) atom type and to calculate the charge parameters for them. Atomic charges were calculated by the AM1-BCC method [59]. The Xleap program was used for the topology files, forcefield force field, and the addition of water molecules and ions to the system, which are necessary for molecular dynamics calculations. The complex was defined as a cubic box-shaped system with x = 20 nm, y = 20 nm, z = 20 nm, TIP3P water model, and ff14SB forcefield were used under periodic boundary conditions. Furthermore, the coligand-receptor was neutralized with 4 chlorine (Cl^-) ions and the PBB-receptor complex structure was neutralized with 3 chlorine (Cl^-) ions (Fig. 11).

The energy minimization of both complex systems was completed with the steepest descent algorithm and 560 steps. The potential energy change of the simulated system was calculated and shown in Fig. 12. It is seen that the potential energy value becomes stable by decreasing and the total energy is negative. It is seen that the potential energy of both systems varies from -4×10^5 kJ/mol to -1.1×10^6 kJ/mol and the total potential energies of the systems are stable around -1.05×10^6 kJ/mol, which is a similar value after 100 steps of the simulation.

After the energy minimization of the system, in the simulations made in the NPT ensemble where the pressure and temperature are kept constant, two complex structures were contacted with a 300 K heat storage

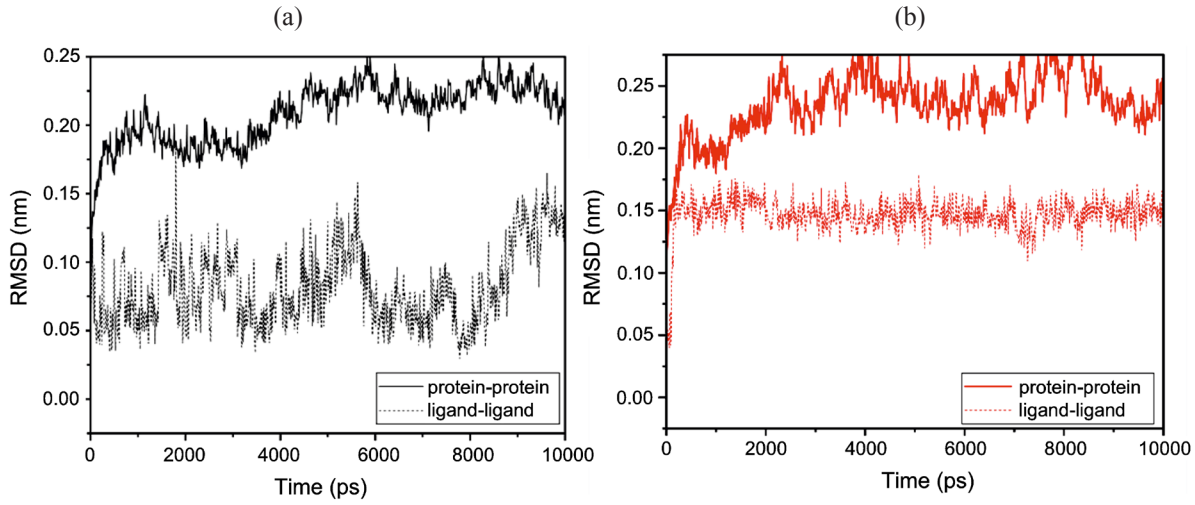

Fig. 13. RMSD plot of protein-protein and ligand-ligand interactions of (a) coligand-protein and (b) PBB-protein complexes.

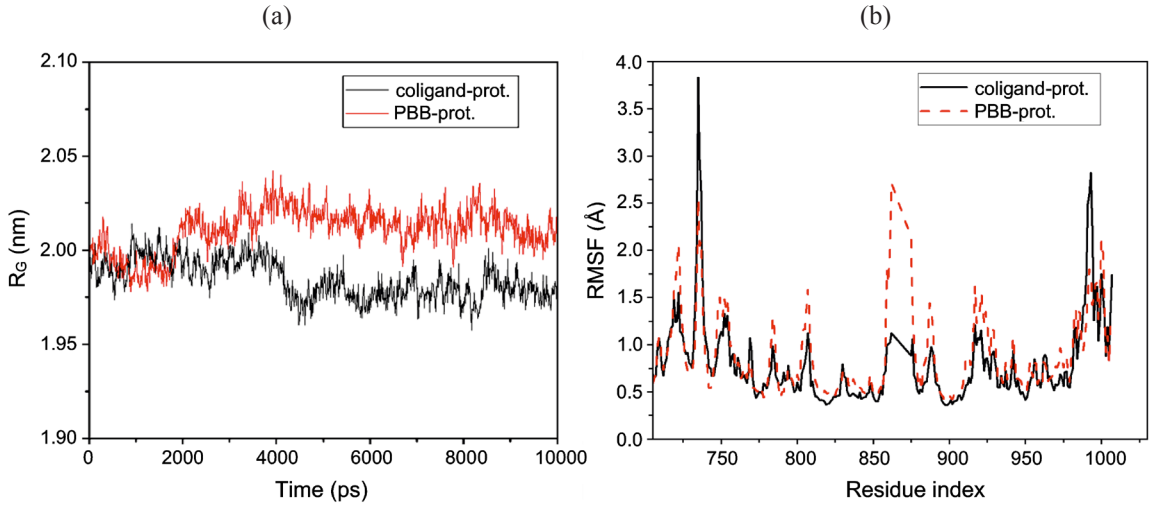

Fig. 14. (a) R_G and (b) RMSF plot of complex structures.

and a pressure thermostat with 1 bar pressure throughout the simulation. In these short MD simulations, temperature and pressure were controlled with v-rescale and Parrinello Rahman thermostats, respectively. The compressibility constant is 4.5×10^{-5} bar^{-1} and the time constant is 2 ps. For van der Waals and short-range Coulomb interactions, the cut-off radius is fixed at 1.4 nm. PME (Particle Mesh Ewald) method was used for long range interactions. Periodic boundary conditions were applied in the simulations and the time step was taken as 1×10^4 ps. Finally, the balanced systems were subjected to MD simulation with the Leap-frog Verlet algorithm. From the simulation results, it was seen that the molecules were stable and the RMSD values were within acceptable (< 2.0 Å) values. In addition, it is seen that the coligand makes large fluctuations around 1 Å inside the receptor, while the (**PBB**) has stable RMSD values of around 1.5 Å (Fig. 13).

The R_G (radius of rotation) of a protein is a measure of its compactness. If a protein is stably folded, it will likely maintain a relatively constant R_G value. If a protein is turned on, its R_G will change over time. In the simulation of both complex structures, we can see that the R_G values do not change after 4000 ns and the protein structures remain stable (Fig. 14a). When the RMSF graphs of the

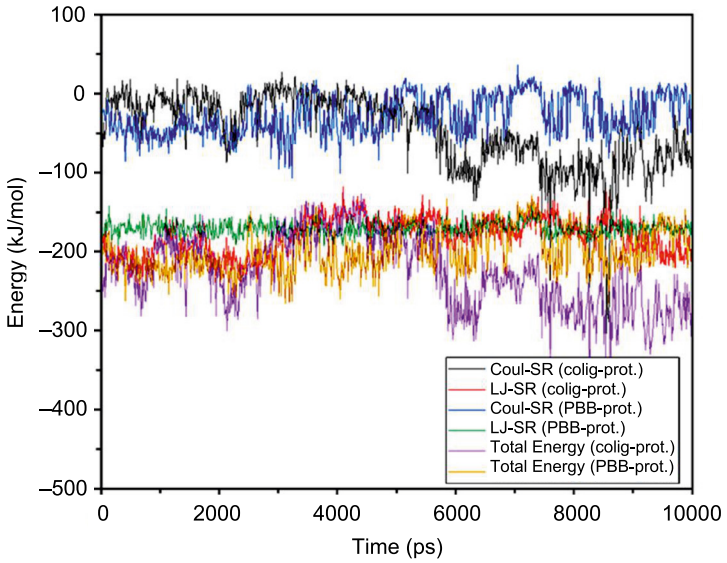

Fig. 15. Short and long-range interaction and total energies of complex structures.

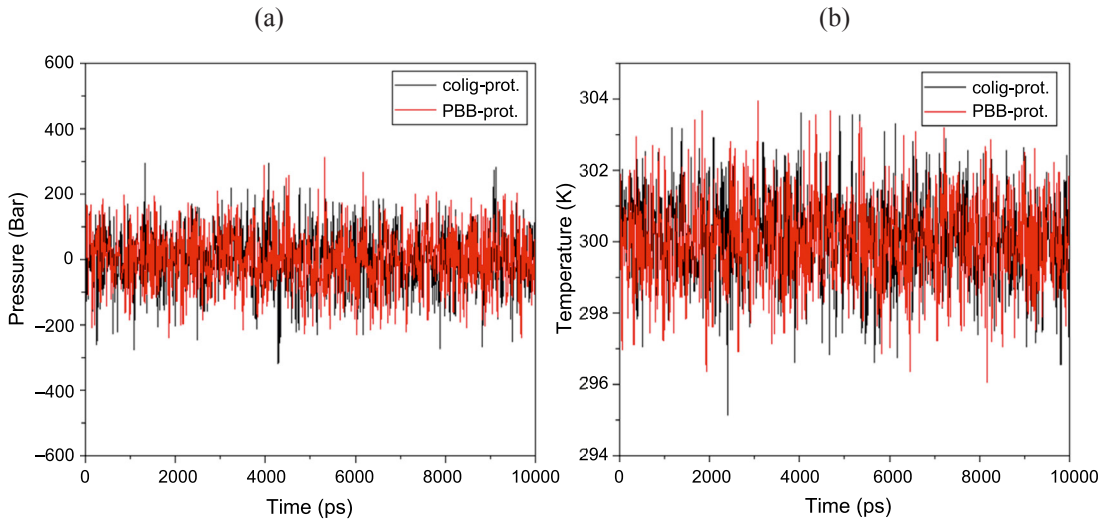

Fig. 16. Pressure and temperature plots of complex structure.

complexes formed by the ligands with the protein were examined, it was observed that the fluctuations of the critical residues of the coligand-protein complex were around 3.6 and 2.6 Å, while the PBB-protein complex was around 2.5 and 2.6 Å (Fig. 14b). These calculations can be cited as an important parameter supporting that the ligands at these sites exhibit stable interactions with the protein binding site.

The interaction energies between the coligand-protein and PBB-protein complexes were measured by the short-range (SR) Coulomb (Coul-SR), and Lennard-Jones (LJ-SR) potentials (Fig. 15). The averages of the LJ-SR and Coul-SR total interaction energies of the coligand-protein complex are –46.88 ± 17 and –179.99 ± 7 kJ/mol, respectively. The averages of the total interaction energies of the PBB-protein complex were calculated as –27.84 ± 5.6 and –170.59 ± 0.9 kJ/mol.

Figure 16 shows the graphs of the time dependent changes in pressure and temperature during 1×10^4 ps. According to both graphs obtained at the equilibrium

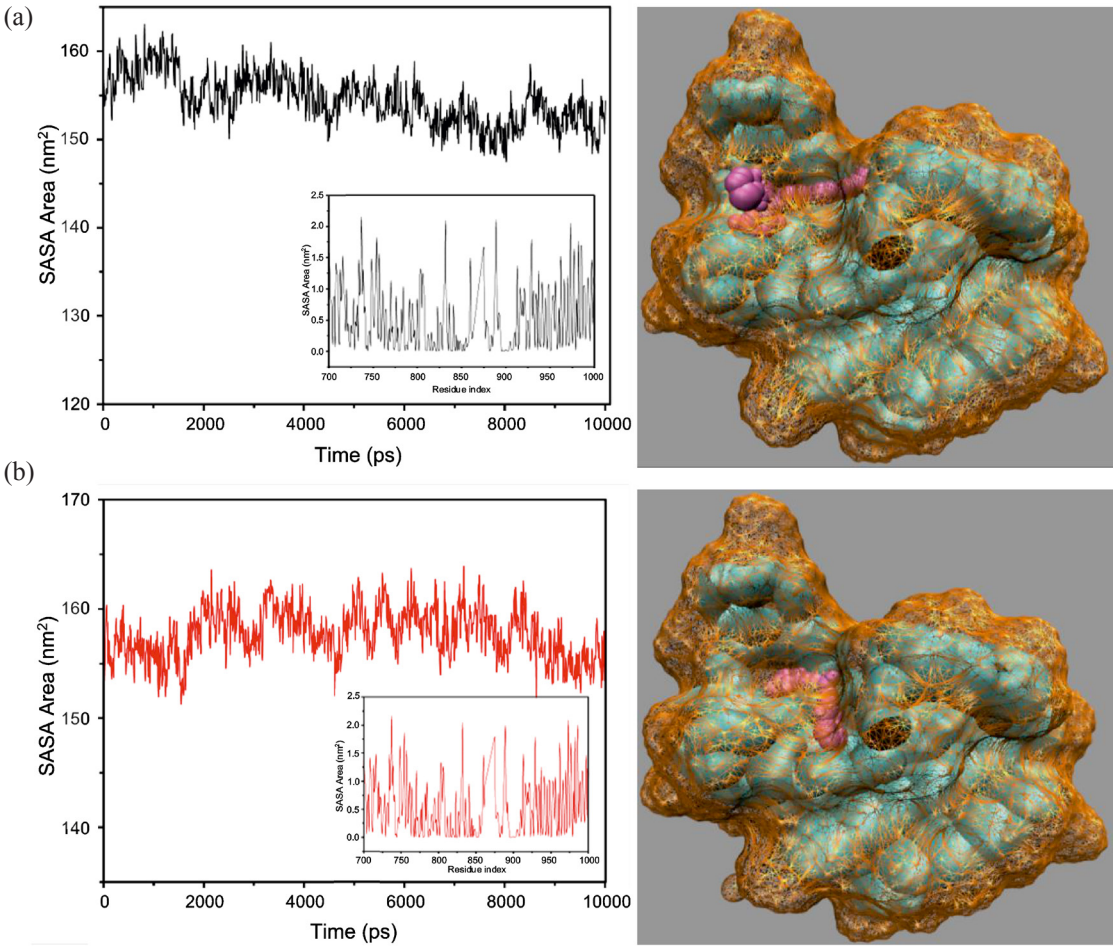

Fig. 17. SASA change and 3D plots of (a) coligand-protein and (b) PBB-protein complexes.

step lasting 1×10^4 ps under constant pressure, constant temperature, and constant molecule number conditions, although there are large oscillations in pressure values during the simulation process, these oscillations are around 1 bar. The average pressure values are 0.73 and 0.90 bar for coligand-protein and PBB-protein complexes respectively. Small oscillations are observed in the temperature values of both complex structures and these oscillations vary around 300 K. The average temperature values are 299.99 and 300.00 K for coligand-protein and PBB-protein complexes, respectively. The pressure-time and temperature-time plots show that the constant pressure and constant temperature values obtained indicate that both systems are in a good equilibrium state.

Since determining the interaction of the system with water can provide information about the dynamic behavior of protein structures, solvent accessible surface area (SASA) analysis was performed for each simulation group. The most effective forces in protein folding are hydrophobic forces. Therefore, in order to see the effect of hydrophobic forces on the systems, total solvent accessible surface areas (SASA) were calculated at 300 K and both time-dependent and contributions from each residue were given together. The 3D SASA was also colored on the protein. From the molecular dynamics (MD) simulations, a decreasing fluctuation of SASA values between 160 and 150 $Å^2$ is observed for the coligand-protein complex structure, while for the PBB-protein complex structure, it fluctuates between 160 and 150 $Å^2$ and increases above 160 $Å^2$ in the range of 2000–8000 ns (Fig. 17). This indicates that the coligand-protein complex structure has less water interaction than the PBB-protein complex,

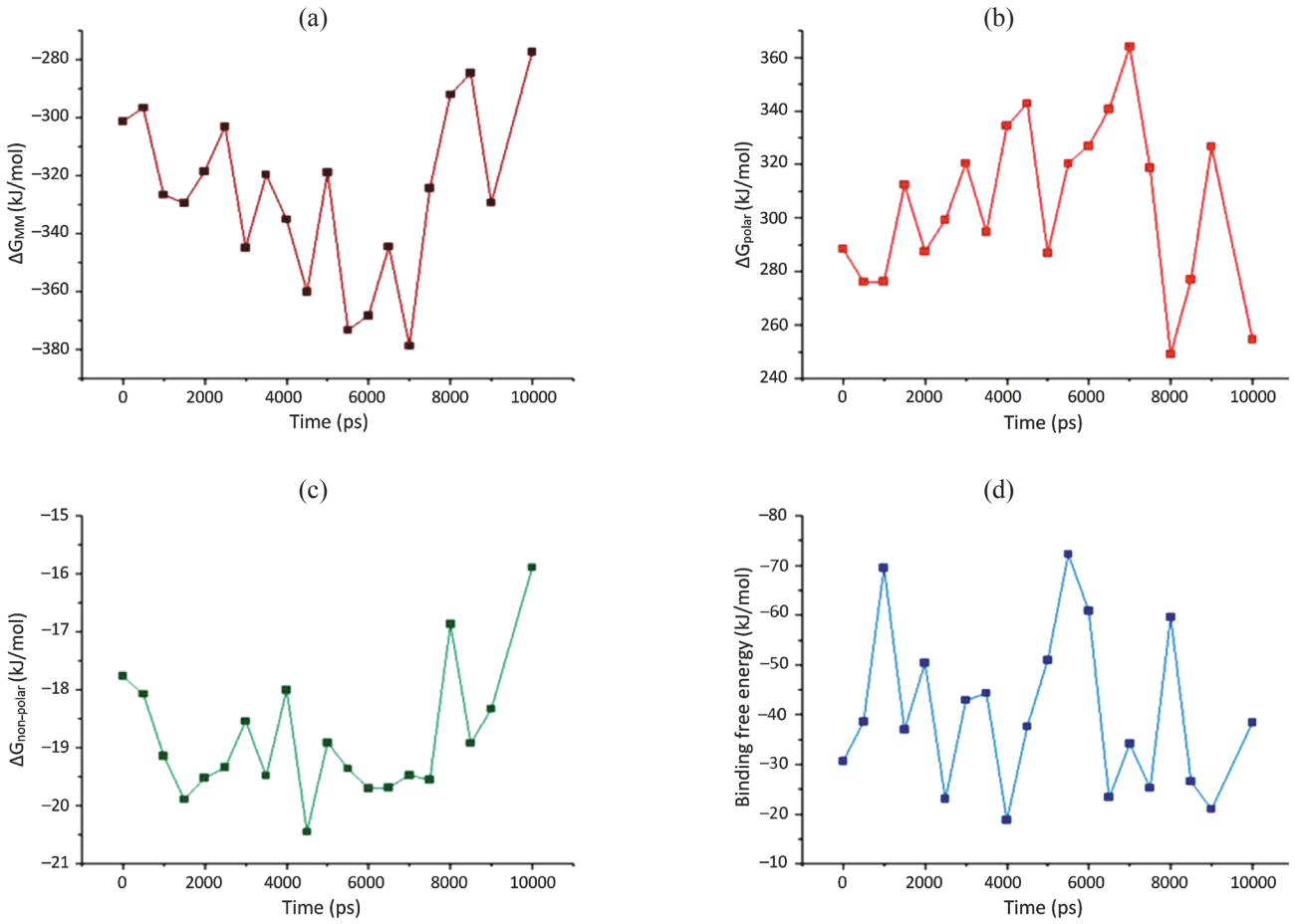

Fig. 18. Energy components of coligand-protein; (a) the potential energy in the vacuum, (b) polar solvation energy, (c) non-polar solvation energy, and (d) binding free energy. ΔG, change in free energy, MM; molecular mechanics.

that is, it is more hydrophobic. In addition, in order to determine the contribution of residues in each protein to hydrophobicity in the simulation, the samples were averaged for the available simulation groups and shown in the graph.

Binding Free Energy Calculations

The reliability of ligand-protein interactions can be measured by determining the binding free energy (ΔG_{bind}). For this, the MM/PBSA (Molecular Mechanics Poisson-Boltzmann Surface Area) [60] approach provides an important explanation for the efficiency of ligand binding to protein [61]. The binding free energies of the ligands between the proteins were performed with the g_mmpbsa module. The binding free energy ΔG_{bind} is given by the following equation (1) [62]:

$$\Delta G_{bind} = \Delta E_{MM} + \Delta G_{polar} + \Delta G_{nonpolar} - T\Delta S, \quad (1)$$

where ΔG_{polar} and $\Delta G_{nonpolar}$ are polar and nonpolar dissolution energies, respectively, and E_{MM} is the molecular mechanical energy from electrostatic (E_{ele}) and Van der Waals (E_{vdw}) contributions. T is the absolute temperature and ΔS is the entropy change. Binding free energies of protein-ligand complexes during 1×10^4 ps in the simulation (Figs. 18 and 19) and the calculated summary energies of the components that make up these energies are listed in Table 6.

According to the results, the binding free energy value of the synthesized (**PBB**) ligand was calculated larger

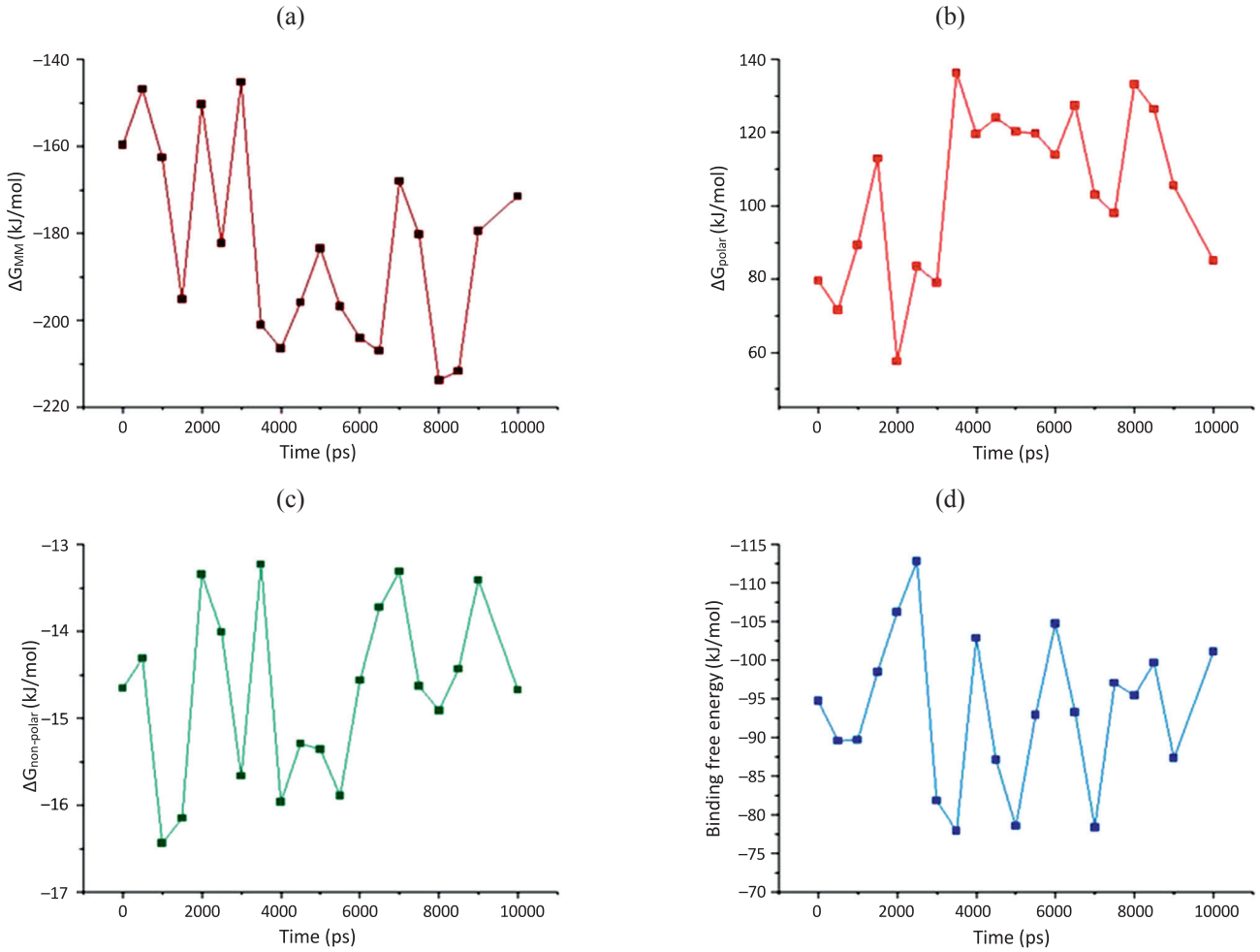

Fig. 19. Energy components of PBB-protein; (a) The potential energy in the vacuum, (b) polar solvation energy, (c) non-polar solvation energy, (d) binding free energy. ΔG, change in free energy; MM, molecular mechanics.

Table 6. Summary energies (kJ/mol) of coligand-protein and PBB-protein

Interaction energies	Coligand-protein	PBB-protein
Van der Waal energy	–209.232 ± 21.798	–180.642 ± 11.463
Electrostatic energy	–118.196 ± 27.026	–9.470 ± 16.230
Polar solvation energy	304.831 ± 33.856	+105.122 ± 22.132
SASA energy	–19.093 ± 1.290	–14.750 ± 0.735
Binding free energy	–41.689 ± 20.746	–99.740 ± 14.748

Table 7. Antioxidant activity of (**PBB**) and standards

Sample	DPPH· (SC_{50}, mg/mL)	FRAP (μM, TEAC)
(**PBB**)	1.8686 ± 0.0030	108.89 ± 1.92
BHT	0.0115 ± 0.0001	N.D.
Trolox	0.0028 ± 0.0000	#

N.D, not detected; #, Trolox was used to constructing a calibration curve used for the calculation of TEAC values.

Table 8. Antibacterial activity values of (**PBB**) with compared antimicrobial agent (inhibition zone, mm)

Compound	Concentration (μg/mL)	Bacteria					
		B. subtilis	*B. megaterium*	*E. feacalis*	*S. aureus*	*E. coli*	*S. typhimurium*
(**PBB**)	500	8	7	7	8	7	–
$C_{19}H_{18}N_4O$	250	–	–	–	–	–	–
Ofloxacin	10 μg/disc	18	20	16	17	16	18

than that of coligand. This indicates that the binding of (**PBB**) ligand to 7JXQ receptor is more stable.

Antioxidant Activity

Antioxidant activity of (**PBB**) was tested by DPPH· radical scavenging, FRAP assays (Table 7), and compared with that of the 3,5-di-tert-4-butylhydroxytoluene (BHT), a commercially used antioxidant. According to the DPPH· result, (**PBB**) has moderate radical scavenging activity with a SC_{50} = 1.8686 ± 0.0030 mg/mL value and the FRAP value is 108.89 ± 1.92 μM TEAC. The antioxidant capacity of (**PBB**) has been demonstrated from molecular modeling calculations performed on C=N nitrogen atoms (electron-donor region, HOMO), which are electron-rich regions, and carbon atoms (electron acceptor region, LUMO) adjacent to the C=O group, which is the electron-withdrawing region.

Antibacterial Activity

Antibacterial activity of (**PBB**) was tested against Gram-positive (*B. subtilis*, *B. megaterium*, and *E. faecalis*) and Gram-negative (*E. coli*, *S. aureus*, and *S. typhimurium*) bacteria using disc diffusion method. The test results are shown at Table 8 as inhibition zone (mm). Compound (**PBB**) showed antibacterial activity at the 500 μg/mL dose against both Gram-positive and Gram-negative bacteria except *S. typhimurium*. As in the interpretation of the antioxidant effect, it is possible to say that the antibacterial effect occurs by interacting with the proteins of the bacteria through the electronegative C=N nitrogen atoms (HOMO) and the carbon atoms adjacent to the carbonyl group (LUMO) of (**PBB**) molecule.

EXPERIMENTAL

Chemistry and apparatus. All chemicals and solvents are of reagent grade and were used without further purification. Elemental analysis data were obtained with a Thermo Finnigan Flash EA 1112 analyzer. Melting point was determined using an Electro thermal melting-point apparatus. NMR spectra were run on a Varian Unity Inova 500 NMR spectrometer in DMSO-d_6. FT-IR spectra were recorded on a Bruker Optics Vertex 70 spectrometer using ATR (Attenuated Total Reflection) techniques. The Electron Spray Ionization-Mass Spectrometry (ESI-MS) analyses were carried out in positive ion modes using a Thermo Finnigan LCQ Advantage MAX LC/MS/MS. Fluorescence spectra were performed on a

Shimadzu RF-5301 PC Spectrofluorophotometer in EtOH ($c = 1 \times 10^{-4}$ mol/L).

Synthesis of 1,5-bis(1*H*-benzimidazol-2-yl)pentan-3-one (PBB). Compound (**PBB**) was synthesized from 0.01 mole of 4-oxopimelic acid (or 4-oxo-heptanedioic acid, 1.74 g) and 0.02 mole of 1,2-phenylenediamine (2.16 g) in 5.5 N HCl (20 mL) according to the literature [49]. Slightly yellow solid; Yield: 72%; mp: 223°C; FT-IR (ATR) ν_{max}, cm^{-1}: 3283 m ν(NH), 3056 m ν(CH_{arom}), 2921 m ν(CH_{aliph}), 1712 s ν(C=O), 1629 m ν(C=N), 1598 m ν(C=C), 1539 m, 1444 m, 1407 m, 1270 m, 1195 m, 1103 m, 821 m, 743 s δ(CH_{arom}), 707 m, 649 m, 432 m; ^{1}H NMR (500 MHz, DMSO-d_6), ppm: 7.46 s (2H, H4 + H7), 7.11 s (2H, H5 + H6), 3.11 d, br (2H, J = 4.1 Hz, Im–C$\underline{H}_2$–CH_2–C=O), 3.06 d, br (2H, J = 4.2 Hz, Im–CH_2–C$\underline{H}_2$–C=O); ^{13}C NMR (125 MHz, DMSO-d_6), ppm: 208.70 (C=O), 155.00 (C2), 122.21 (C9), 121.87 (C8), 121.55 (C4 + C7), 115.07 (C5 + C6), 39.84 (Im–$\underline{C}H_2$–CH_2–C=O), 23.28 (Im–CH_2–$\underline{C}H_2$–C=O); ESI-MS, %: *m/z* 319.4 (100, $[M + H]^+$); *m/z* 320.5 (24.6, $[M + 2H]^+$). Fluorescence spectra (in EtOH, nm): 394 m, 421 m, br, 458 m, br; $C_{19}H_{18}N_4O$ (318.37 g/mol); Calculated, %: C, 71.68; H, 5.70; N, 17.60; Found, %: C, 71.56; H, 5.81; N, 17.53.

X-ray diffraction analysis. Suitable crystal of (**PBB**) was selected for data collection which was performed on a D8-QUEST diffractometer equipped with a graphite-monochromatic Mo–K_α radiation at 296 K. The structure was solved by direct methods using SHELXS-2013 [63] and refined by full-matrix least-squares methods on F^2 using SHELXL-2013 [64]. All non-hydrogen atoms were refined with anisotropic parameters. The H atoms were located from different maps and then treated as riding atoms with C–H distance of 0.93–0.97 Å. The other H atoms were located in a difference map refined freely. The following procedures were implemented in our analysis: data collection: Bruker APEX2 [65]; program used for molecular graphics were as follow: MERCURY programs [66]; software used to prepare material for publication: WinGX [67]. Details of data collection and crystal structure determinations are given in Table 1.

Computational details. The calculations of the parameters used for the optimization of (**PBB**) and coligand (JBJ-09-063) compounds and the determination of the electrophilic and nucleophilic active sites of the (**PBB**) compound were obtained using the Gaussian 09 program [68], the B3LYP [69, 70] theory and the 6-311g(d,p) [71, 72] basis set. The obtained results were visualized using the program GaussView 5 [72] (Fig. 2). Docking simulations of ligands and protein structures were performed using chimera [57] and AutoDock Vina software [73]. Using the data obtained as a result of the docking simulation, MD simulations were performed with the help of "GROMACS" software [74] and Binding Free Energies calculations of complex structures were performed with the g_mmpbsa module [62].

Antioxidant activity determination. 1,1-Diphenyl-2-picrylhydrazyl (DPPH·) radical scavenging activity: radical scavenging activity was tested by using the commonly used DPPH· radical scavenging activity [75]. Each of the concentrations of the samples were mixed with 100 μM methanolic DPPH· solution in an equal volume (750 μL) and kept for 50 min at room temperature. Then, all experimental setups were spectrophotometrically measured at 517 nm. The concentrations corresponding to the absorbances found were plotted, and the 50% scavenging concentration (SC_{50}) values were calculated in mg/mL. Low SC_{50} values indicated higher radical cleaning potential.

Ferric Reducing/Antioxidant power (FRAP) method: in FRAP method, 50 μL of each tested samples was mixed with 1.5 mL of FRAP reagent and after 20 min the absorbance was spectrophotometrically measured at 595 nm. The absorbance of all tubes was compiled against pure water. The ferric reducing activity of each sample was determined by the calibration graph obtained using trolox in the range of 31.25–1000 μM and the micromolar trolox equivalent antioxidant capacity (TEAC) was determined [76].

Antibacterial activity determination. The solution of (**PBB**) was prepared with DMSO at 1000, 500, 250, 125 μg/mL concentrations. The used microorganisms were three Gram-positive (*B. subtilis* ATCC 6633, *B. mega-*

terium ATCC 19213, and *E. faecalis* ATCC 29212) and three Gram-negative (*E. coli* ATCC 25922, *S. aureus* ATCC 29213, and *S. typhimurium* ATCC 14028) bacteria. The studied bacteria were diluted with Mueller Hinton Broth (MHB) containing 10^6 cfu/mL. DMSO and Ofloxacin (10 μg/disc) were used negative control and positive control, respectively. Mueller Hinton Agar (MHA) was used as the medium. Antibacterial activity was evaluated by disc diffusion method described by Karaçelik et al. [77]. Each bacterial solution was separately spread on MHA medium in sterile conditions. Then, 6 mm standard discs were individually impregnated with 10 μL of each concentration of tested compounds and were and placed on MHA. The prepared experimental setups were incubated at 37°C and after 24 h the diameters of the transparent inhibition zone around the standard discs, on which the compounds were impregnated, were measured and recorded. Each experiment was performed in triplicate.

CONCLUSIONS

In this study, a new symmetric ketonic bis-benzimidazole derivative, 1,5-bis(1*H*-benzimidazol-2-yl)-pentan-3-one (**PBB**), was synthesized and characterized by spectroscopic techniques and X-ray crystal structure. (**PBB**) molecules are connected by N–H···N hydrogen bonds formed as a result of the interaction between NH hydrogen and C=N nitrogen atoms. There are also C–H···π and π···π interactions between the (**PBB**) molecules. Molecular modelling techniques and approaches were used to ensure that (**PBB**) synthesized in this study could be a reliable drug-like ligand, ligand-protein interactions were studied in detail with molecular dynamic (MD) simulation techniques applied at the molecular level, and trajectory analyses after MD were discussed. As a result of MD simulation, allosteric inhibitor JBJ-09-063-like molecule has been revealed as a new and reliable EGFR inhibitor with the feature of being a drug. The total antioxidant capacity (as TEAC value) and free radical scavenging activity of (**PBB**) was investigated by ferric reducing antioxidant power (FRAP) and 1,1-diphenyl-2-picrylhydrazyl (DPPH) methods, respectively, and the results showed that it has a moderate inhibition effect. In addition, antibacterial activity of (**PBB**) was tested against Gram-positive and Gram-negative bacteria using disc diffusion method. It was observed that the title compound showed moderate activity in both areas. According to the molecular modelling calculations, the antioxidant and antibacterial activities of (**PBB**) result from the electrophilic and nucleophilic interactions of its electron-rich C=N nitrogen atoms and electron-withdrawing carbon atoms adjacent to the C=O group with the proteins of the target molecules.

FUNDING

Computing resources used in this work were provided by the National Center for High Performance Computing of Turkey (UHeM) under grant no. 1012982022.

This work was supported by the Scientific Research Projects Coordination Unit of Istanbul University-Cerrahpaşa.

ETHICS APPROVAL AND CONSENT TO PARTICIPATE

This article does not contain any studies involving patients or animals as test objects.

Informed consent was not required for this article.

CONFLICT OF INTEREST

No conflicts of interest was declared by the authors.

AUTHOR CONTRIBUTION

The author AT—selected the literature data on the review topic, synthesis, and spectral characterization; the author TK—computational studies and discussions; the author OŞ—X-ray single crystal data studies; the author DNÇ—antioxidant test and evaluation; the author AAK—antibacterial tests and evaluation.

All authors participated in the discussions.

DATA AVAILABILITY

The data that support the findings of this study are available from the corresponding author upon reasonable request.

SUPPLEMENTARY INFORMATION

The online version contains supplementary material available at https://doi.org/10.1134/S1068162024040253

REFERENCES

1. Brishty, S.R., Hossain, M.J., Khandaker, M.U., Faruque, M.R.I., Osman, H., and Rahman, S.M., *Front. Pharmacol.*, 2021, vol.12, Article ID: 762807. https://doi.org/10.3389/fphar.2021.762807
2. Wang, M., Han, X., and Zhou, Z., *Exp. Opin. Ther. Pat.*, 2015, vol. 25, pp. 595–612. https://doi.org/10.1517/13543776.2015.1015987
3. Fei, F. and Zhou, Z., *Exp. Opin. Ther. Pat.*, 2013, vol. 23, pp. 1157–1179. https://doi.org/10.1517/13543776.2013.800857
4. Kamanna, K., *Chemistry and Applications of Benzimidazole and its Derivatives*, Marinescu, M., Ed., 2019, Ch. 5,, IntechOpen, London, UK.
5. Akande, A.A., Salar, U., Khan, K.M., Syed, S., Aboaba, S.A., Chigurupati, S., Wadood, A., Riaz, M., Taha, M., Bhatia, S., Kanwal, Shamim, S., and Perveen, S., *ACS Omega*, 2021, vol. 6, pp. 22726–22739. https://doi.org/10.1021/acsomega.1c03056
6. Sun, T., Li, K., Lai, Y., Chen, R., and Wu, H., *Acta Cryst.*, 2010, vol. E66, p. m1058. https://doi.org/10.1107/s1600536810030357
7. Holland, P.L. and Tolman, W.B., *J. Amer. Chem. Soc.*, 2000, vol. 122, pp. 6331–6332. https://doi.org/10.1021/ja001328v
8. Ramla, M.M., Omar, M.A., Tokuda, H., and El-Diwani, H.I., *Bioorg. Med. Chem.*, 2007, vol. 15, pp. 6489–6496. https://doi.org/10.1016/j.bmc.2007.04.010
9. Navarrete-Vázquez, G., Rojano-Vilchis, M.M, Yépez-Mulia, L., Meléndez, V., Gerena, L., Hernández-Campos, A., Castillo, R., and Hernández-Luis, F., *Eur. J. Med. Chem.*, 2006, vol. 41, pp. 135–141. https://doi.org/10.1016/j.ejmech.2005.09.001
10. Rivara, M., Zuliani, V., Cocconcelli, G., Morini, G., Comini, M., Rivara, S., Mor, M., Bordi, F., Barocelli, E., Ballabeni, V., Bertoni, S., and Plazzi, P.V., *Bioorg. Med. Chem.*, 2006, vol. 14, pp. 1413–1424. https://doi.org/10.1016/j.bmc.2005.09.063
11. Safonov, I.G., Heerding, D.A., Keenan, R.M., Price, A.T., Erickson-Miller, C.L., Hopson, C.B., Levin, J.L., Lord, K.A., and Tapley, P.M., *Bioorg. Med. Chem. Lett.*, 2006, vol. 16, pp. 1212–1216. https://doi.org/10.1016/j.bmcl.2005.11.096
12. Tavman, A., *Rev. Inorg. Chem.*, 2002, vol. 22, pp. 41–51. https://doi.org/10.1515/revic.2002.22.1.41
13. Tavman, A., *Main Group Met. Chem.*, 2003, vol. 26, pp. 229–235. https://doi.org/10.1515/mgmc.2003.26.4.229
14. Tavman, A., *Rev. Inorg. Chem.*, 2005, vol. 25, pp. 377–383. https://doi.org/10.1515/revic.2005.25.4.377
15. Tavman, A., *Russ. J. Inorg. Chem.*, 2005, vol. 50, pp. 1341–1345.
16. Tavman, A., *J. Serb. Chem. Soc.*, 2006, vol. 71, pp. 521–528. https://doi.org/10.2298/jsc0605521t
17. Tavman, A. and Cinarli, A., *Inorg. Chim. Acta*, 2014, vol. 421, pp. 481–488. https://doi.org/10.1016/j.ica.2014.07.036
18. Tavman, A., Gürbüz, D., and Cinarli, A., *J. Serb. Chem. Soc.*, 2018, vol. 83, pp. 1099–1112. https://doi.org/10.2298/jsc180123046t
19. Isele, K., Broughton, V., Matthews, C.J., Williams, A.F., Bernardinelli, G., Franz, P., and Decurtins, S., *J. Chem. Soc. Dalton Trans.*, 2002, vol. 2002, pp. 3899–3905. https://doi.org/10.1039/b203229e
20. Lavrenko, P., Okatova, O., Strelina, I., Bruma M., and Schulz, B., *Polymer*, 2003, vol. 44, pp. 2919–2925. https://doi.org/10.1016/s0032-3861(03)00172-1
21. Fukushima, K., Jones, G.O., Horn, H.W., Rice, J.E., Kato, T., and Hedrick, J.L., *Polym. Chem.*, 2020, vol. 11, pp. 4904–4913. https://doi.org/10.1039/d0py00436g
22. Tavman, A., Birteksöz, S., and Otük, G., *Folia Microbiol.*, 2005, vol. 50, pp. 467–472. https://doi.org/10.1007/bf02931431

23. Kücükbay, H., Durmaz, B., Okyucu, N. and Günal, S., *Folia Microbiol.*, 2003, vol. 48, pp. 679–681. https://doi.org/10.1007/bf02993478
24. Kücükbay, H., Durmaz, R., Okuyucu, N., Günal, S. and Kazaz, C., *Arzneimittelforschung*, 2004, vol. 54, pp. 64–68. https://doi.org/10.1055/s-0031-1296938
25. Agh-Atabay, N.M., Neshat, A., Karabiyik, T., Somer, M., Haciu, D., and Dülger, B., *Eur. J. Med. Chem.*, 2007, vol. 42, pp. 205–213. https://doi.org/10.1016/j.ejmech.2006.09.023
26. Hebishy, A.M., Abdelfattah, M.S., Elmorsy, A., and Elwahy, A.H.M., *J. Het. Chem.*, 2020, vol. 57, pp. 2256–2270. https://doi.org/10.1002/jhet.3947
27. Bansal, Y., Kaur, M., and Bansal, G., *Mini Rev. Med. Chem.*, 2019, vol. 19, pp. 624–646. https://doi.org/10.2174/1389557517666171101104024
28. Sindelar, Z. and Kopel, P., *Inorganics*, 2023, vol. 11, Article ID: 113. https://doi.org/10.3390/inorganics11030113
29. Ouaket, A., Addoum, B., El Khalfi, B., Soukri, A., Knouzi, N., and Berrada, M., *Mor. J. Chem.*, 2021, vol. 9, pp. 250–259. https://doi.org/10.48317/imist.prsm/morjchem-v9i2.20868
30. Ouaket, A., Moughaoui, F., Laaraibi, A., Hamdouch, S., Berrada, M., and Knouzi, N., *Mediterr. J. Chem.*, 2019, vol. 8, pp. 103–107. https://doi.org/10.13171/mjc8219041101ao
31. Yildiz, U., *J. Heterocycl. Chem.*, 2020, vol. 57, pp. 4007–4012. https://doi.org/10.1002/jhet.4110
32. Mao, S., Shen, K., Shi, X., Wu, H., Han, X., Li, C., and Huang, G., *Inorg. Chim. Acta*, 2018, vol. 471, pp. 82–90. https://doi.org/10.1016/j.ica.2017.10.038
33. Wu, H., Yang, Z., Wang, F., Peng, H., Zhang, H., Wang, C., and Wang, K., *J. Photochem. Photobiol. B*, 2015, vol. 148, pp. 252–261. https://doi.org/10.1016/j.jphotobiol.2015.04.014
34. Wu, H., Kou, F., Jia, F., Liu, B., Yuan, J., and Bai, Y., *Z. Anorg. Allg. Chem.*, 2012, vol. 638, pp. 443–450. https://doi.org/10.1002/zaac.201100354
35. Wang, C., Wu, Y., Qu, Y., Zhao, K., Xu, J., Xia, X., and Wu, H., *Transit. Met. Chem.*, 2020, vol. 45, pp. 523–529. https://doi.org/10.1007/s11243-020-00405-9
36. Wu, H., Kou, F., Jia, F., Liu, B., Yuan, J., and Bai, Y., *Bioinorg. Chem. Appl.*, 2011, vol. 2011, Article ID: 105431. https://doi.org/10.1155/2011/105431
37. Wu, H., Kou, F., Jia, F., Liu, B., Yuan, J., and Bai, Y., *J. Photochem. Photobiol. B*, 2011, vol. 105, pp. 190–197. https://doi.org/10.1016/j.jphotobiol.2011.09.001
38. Xia, X., Xia, L., Zhang, G., Xu, J., Wang, C., Wu, Y., Zhao, K., and Wu, H., *J. Coord. Chem.*, 2020, vol. 73, pp. 3322–3331. https://doi.org/10.1080/00958972.2020.1857746
39. Wu, H., Wang, H., Wang, X., Pan, G., Shi, F., Zhang, Y., Bai, Y., and Kong, J., *New J. Chem.*, 2014, vol. 38, pp. 1052–1061. https://doi.org/10.1039/c3nj01145c
40. Zhang, H., Xu, Y., Wu, H., Aderinto, S.O., and Fan, X., *RSC Adv.*, 2016, vol. 6, pp. 83697–83708. https://doi.org/10.1039/c6ra09733b
41. Wu, H., Yuan, J., Bai, Y., Pan, G., Wang, H., Kong, J., Fan, X., and Liu, H., *Dalton Trans.*, 2012, vol. 41, pp. 8829–8838. https://doi.org/10.1039/c2dt30512g
42. Tavman, A., *Main Group Met. Chem.*, 2012, vol. 35, pp. 81–90. https://doi.org/10.1515/mgmc-2012-0009
43. Miranda, F.S., Menezes, F.G., Vicente, J., Bortoluzzi, A.J., Zucco, C., Neves, A., and Goncalves, N.S., *J. Mol. Struct.*, 2009, vol. 938, pp. 1–9. https://doi.org/10.1016/j.molstruc.2009.08.031

44. Bitler, C.M., Wood, P., Anstine, D., Meyer-Franke, A., Zhao, Q., and Khan, M., US Patent application, 2004, 20040072862 A1.
45. Bitler, C.M., Wood, P., Anstine, D., Meyer-Franke, A., Zhao, Q., and Khan, M., WO Patents, 2000, 2000075117.
46. Ramirez, E., Martinez, E., Hernández-Ortega, S., Flores-Alamo, M., and Castillo, I., *Inorg. Chim. Acta*, 2018, vol. 481, pp. 181–188. https://doi.org/10.1016/j.ica.2017.08.039
47. Yao, H.C., Li, M.M., Yang, G.S., Li, Z.J., and Zhu, Y., *Inorg. Chim. Acta*, 2007, vol. 360, pp. 3959–3964. https://doi.org/10.1016/j.ica.2007.04.042
48. Gorun, S.M., Stibrany, R.T., Katritzky, A.R., Slawinski, J.J., Faid-Allah, H., and Brunner, F., *Inorg. Chem.*, 1996, vol. 35, pp. 3–4. https://doi.org/10.1021/ic950698v
49. Shriner, R.L. and Upson, R.W., *J. Amer. Chem. Soc.*, 1941, vol. 63, pp. 2277–2278. https://doi.org/10.1021/ja01853a506
50. Ouaket, A., Chraka, A., Raissouni, I., El-Amrani, M.A., Berrada, M., and Knouzi, N., *J. Mol. Struct.*, 2022, vol. 1259, Article ID: 132729. https://doi.org/10.1016/j.molstruc.2022.132729
51. Mosquera, M., Rodriguez, M.C.R., and Rodriguez-Prieto, F., *J. Phys. Chem. A*, 1997, vol. 101, pp. 2766–2772. https://doi.org/10.1021/jp9626834
52. Rodriguez-Prieto, F., Penedo, J.C., and Mosquera, M., *J. Chem. Soc. Faraday Trans.*, 1998, vol. 94, pp. 2775–2782. https://doi.org/10.1039/a803209b
53. Mahalakshmi, G. and Balachandran, V., *Spectrochim. Acta A*, 2015, vol. 135, pp. 321–334. https://doi.org/10.1016/j.saa.2014.06.157
54. He, J., He, H., Cai, M., Zhao, F., and He, H., *J. Mol. Struct.*, 2020, vol. 1199, Article ID: 126991. https://doi.org/10.1016/j.molstruc.2019.126991
55. Ayati, A., Emami, S., Moghimi, S., and Foroumadi, A., *Future Med. Chem.*, 2019, vol. 11, pp. 1929–1952. https://doi.org/10.4155/fmc-2018-0416
56. To, C., Beyett, T.S., Jang, J., Feng, W.W., Bahcall, M., Haikala, H.M., Shin, B.H., Heppner, D.E., Rana, J.K., Leeper, B.A., Soroko, K.M., Poitras, M.J., Gokhale, P.C., Kobayashi, Y., Wahid, K., Kurppa, K.J., Gero, T.W., Cameron, M.D., Ogino, A., Mushajiang, M., Xu, C., Zhang, Y., Scott, D.A., Eck, M.J., Gray, N.S., and Jänne, P.A., *Nat. Cancer*, 2022, vol. 3, pp. 402–417. https://doi.org/10.1038/s43018-022-00351-8
57. Pettersen, E.F., Goddard, T.D., Huang, C.C., Couch, G.S., Greenblatt, D.M., Meng, E.C., and Ferrin, T.E., *J. Comput. Chem.*, 2004, vol. 25, pp. 1605–1612. https://doi.org/10.1002/jcc.20084
58. Case, D.A., Ben-Shalom, I.Y., Brozell, S.R., Cerutti, D.S., Cheatham, T. E., III, Cruzeiro, V.W.D., Darden, T.A., Duke, R.E., Ghoreishi, D., Gilson, M.K., Gohlke, H., Goetz, A.W., Greene, D., Harris, R., Homeyer, N., Huang, Y., Izadi, S., Kovalenko, A., Kurtzman, T., Lee, T.S., LeGrand, S., Li, P., Lin, C., Liu, J., Luchko, T., Luo, R., Mermelstein, D.J., Merz, K.M., Miao, Y., Monard, G., Nguyen, C., Nguyen, H., Omelyan, I., Onufriev, A., Pan, F., Qi, R., Roe, D.R., Roitberg, A., Sagui, C., Schott-Verdugo, S., Shen, J., Simmerling, C.L., Smith, J., Salomon-Ferrer, R., Swails, J., Walker, R.C., Wang, J., Wei, H., Wolf, R.M., Wu, X., Xiao, L., York, D.M., and Kollman, P.A., *AMBER 2018*, 2018, University of California, San Francisco, USA.
59. Wang, J., Wolf, R.M., Caldwell, J.W., Kollman, P.A., and Case, D.A., *J. Comput. Chem.*, 2004, vol. 25, pp. 1157–1174. https://doi.org/10.1002/jcc.20035
60. Kollman, P.A., Massova, I., Reyes, C., Kuhn, B., Huo, S.H., Chong, L., Lee, M., Lee, T., Duan, Y., Wang, W., Donini, O., Cieplak, P., Srinivasan, J., Case, D.A., and Cheatham, T.E., *Acc. Chem. Res.*, 2000, vol. 33, pp. 889–897. https://doi.org/10.1021/ar000033j
61. Yang, Z., Wu, F., Yuan, X., Zhang, L., and Zhang, S., *J. Mol. Graph. Model.*, 2016, vol. 65, pp. 27–34. https://doi.org/10.1016/j.jmgm.2016.02.006

62. Kumari, R., Kumar, R., Consortium, O.S.D.D., and Lynn, A., *J. Chem. Inf. Model.*, 2014, vol. 54, pp. 1951–1961. https://doi.org/10.1021/ci500020m
63. Sheldrick, G.M., *Acta Cryst. A*, 2008, vol. 64, pp. 112–122. https://doi.org/10.1107/s0108767307043930
64. Sheldrick, G.M., *Acta Cryst. C*, 2015, vol. 71, pp. 3–8. https://doi.org/10.1107/s2053229614024218.
65. *APEX2*, Bruker AXS, Inc., 2013, Madison, Wisconsin USA.
66. Macrae, C.F., Bruno, I.J., Chisholm, J.A., Edgington, P.R., McCabe, P., Pidcock, E., Rodriguez-Monge, L., Taylor, R., Van De Streek, J., and Wood, P.A., *J. Appl. Cryst*., 2008, vol. 41, pp. 466–470. https://doi.org/10.1107/S0021889807067908
67. Farrugia, L.J., *J. Appl. Cryst.*, vol. 45, pp. 849–854. https://doi.org/10.1107/s0021889812029111
68. Frisch, M.J., Trucks, G.W., Schlegel, H.B., Scuseria, G.E., Robb, M.A., Cheeseman, J.R., Scalmani, G., Barone, V., Petersson, G.A., Nakatsuji, H., Li, X., Caricato, M., Marenich, A., Bloino, J., Janesko, B.G., Gomperts, R., Mennucci, B., Hratchian, H.P., Ortiz, J.V., Izmaylov, A.F., Sonnenberg, J.L., Williams-Young, D., Ding, F., Lipparini, F., Egidi, F., Goings, J., Peng, B., Petrone, A., Henderson, T., Ranasinghe, D., Zakrzewski, V.G., Gao, J., Rega, N., Zheng, G., Liang, W., Hada, M., Ehara, M., Toyota, K., Fukuda, R., Hasegawa, J., Ishida, M., Nakajima, T., Honda, Y., Kitao, O., Nakai, H., Vreven, T., Throssell, K., Montgomery, Jr., J.A., Peralta, J.E., Ogliaro, F., Bearpark, M., Heyd, J.J., Brothers, E., Kudin, K.N., Staroverov, V.N., Keith, T., Kobayashi, R., Normand, J., Raghavachari, K., Rendell, A., Burant, J.C., Iyengar, S.S., Tomasi, J., Cossi, M., Millam, J.M., Klene, M., Adamo, C., Cammi, R., Ochterski, J.W., Martin, R.L., Morokuma, K., Farkas, O., Foresman, J.B., and Fox, D.J., *Gaussian 09, Revision a.02*, Gaussian, Inc., 2009, Wallingford, CT 200.
69. Becke, A.D., *J. Chem. Phys.*, 1993, vol. 98, pp. 5648–5656. https://doi.org/10.1063/1.462066
70. Lee, C., Yang, W., and Parr, R.G., *Phys. Rev. B*, 1998, vol. 37, pp. 785–789. https://doi.org/10.1103/physrevb.37.785
71. Foresman, J.B. and Frisch, A., 1996, *Exploring Chemistry with Electronic Structure Methods: A Guide to using Gaussian*.
72. Dennington, R., Keith, T., Millam, J., Eppinnett, K., Hovell, W.L., and Gilliland, R., *GaussView5.0.8*, 2008. https://www.gaussian.com
73. Trott, O. and Olson, A.J., *J. Comput. Chem.*, 2010, vol. 31, pp. 455–461. https://doi.org/10.1002/jcc.21334
74. Abraham, M.J., Murtola, T., Schulz, R., Páll, S., Smith, J.C., Hess, B., and Lindahl, E., *SoftwareX*, 2015, vol. 1–2, pp. 19–25. https://doi.org/10.1016/j.softx.2015.06.001
75. Brand-Williams, W., Cuvelier, M.E., and Berset, C., *Food Sci. Technol.*, 1995, vol. 28, pp. 25–30. https://doi.org/10.1016/s0023-6438(95)80008-5
76. Benzie, I.F.F. and Strain, J.J., *Anal. Biochem.*, 1996, vol. 239, pp. 70–76. https://doi.org/10.1006/abio.1996.0292
77. Karaçelik, A.A., Efe, D., Çakır, V., and Bıyıklıoğlu, Z., *JIST*, 2021, vol. 11, pp. 1302–1310. https://doi.org/10.21597/jist.804539